2017-12

Annual prediction of shoreline erosion and subsequent recovery

Mikhalenko, Natalia

10.1016/j.coastaleng.2017.09.008
Coastal Engineering
Elsevier

Annual Forecasting of Extreme Shoreline Erosion and Subsequent Recovery

Mark A. Davidson[1], Ian L. Turner[2], Kristen D. Splinter[2] and Mitchel D. Harley[2]

Affiliations:

1. Coastal Processes Research Group, Plymouth University. (Corresponding Author)
2. Water Research Laboratory, School of Civil and Environmental Engineering, UNSW Sydney.

Abstract

Prediction of the potential impact of an extreme storm-sequence on coastal resilience and the subsequent rate of post-storm recovery is a fundamental goal for coastal scientists, engineers and managers alike. This paper presents a methodology for forecasting shoreline change over annual time-scales, including the prediction of the potential impact of storm sequences and the subsequent post-storm recovery. The methodology utilises an archive of measured or modelled wave data to produce multiple ($\approx 10^3$) synthetic hydrodynamic forcing time-series to drive an equilibrium shoreline model in a Monte Carlo simulation. A Generalised Extreme Value (GEV) analysis is conducted on the resulting shoreline forecasts in order to evaluate the magnitude of shoreline displacements for predefined return probabilities. Three shoreline displacement bands are defined in a 'traffic light' system, to aid the interpretation of results; a green (normal) band characterising shoreline responses within the typical annual recurrence probability, an amber (high) band defining *events* with recurrence probabilities outside the annual recurrence threshold but within 1/100 of this value, and a red (extreme) band designed to encompass the limit of the shoreline forecasts. The methodology was tested on two field sites with distinctly contrasting wave climates and tidal regime. The first was Perranporth in the UK with a strong seasonal variability in both the wave climate and shoreline response. The second was Narrabeen, Australia, with a much smaller seasonal variability and more storm-dominated wave climate and shoreline response. In both cases an equilibrium shoreline model (ShoreFor) was calibrated using measured shoreline data and complementary wave data. The forecasting methodology was found to be mildly sensitive to the temporal range of the wave data used, with at least 15-years of data required to achieve consistent classification of the magnitude of storm erosion and recovery. Two extreme storm sequences were targeted to test the forecasting methodology, the Pasha Bulker storm sequence recorded at

Narrabeen in June 2007 and the extreme storm sequence which impacted the UK during the winter period of 2013/14. All wave and shoreline time-series recorded in this period were left unseen in model calibrations and subsequent forecasts, in order to provide a rigorous test of the methodology. In all cases the forecasting approach presented here was able to predict both storm erosion and subsequent recovery and give a clear indication of the intensity of the shoreline displacement. Both storm sequences studied had shoreline displacements with occurrence probabilities of ≈1/1200 and rapid post-storm recovery rates. The impact of extreme storms on shoreline recession and subsequent post storm recovery is predictable at these energetic cross-shore transport dominated sites, promising the potential for a new coastal management tool.

1. Introduction

Arguably the 'holy grail' for coastal scientists and engineers is to derive sufficient knowledge and understanding of coastal systems to be able to forecast coastal erosion and accretion with a level of confidence and lead time to permit effective coastal management decisions to be made regarding the use, development and protection of coastal environments. Important coastal management questions addressed here are: What are the potential storm impacts on the coastline? Will the coast recover from the prior violent storm(s) and how long will this recovery take?

In spite of the development of sophisticated process models with demonstrable skill in hindcasting coastal hydrodynamics, the complexities and non-linearity of sediment transport and morphodynamic processes mean that our ability to hindcast (let alone forecast) coastal erosion and recovery at a seasonal time-scale remains limited at the present time. Indeed, our ability to forecast beach recovery with physics-based models has proved to be particularly illusive [1, 2]. The forecast horizon of these detailed process-models is limited not only by computing speed but also their long-term stability and model skill [3].

Common coastal state indicators used by managers to assess the current health of the coastline and resilience to coastal erosion and flooding frequently include some measure of beach volume or shoreline position [4, 5]. So, in this contribution, a 'simpler' methodology appropriate to forecasting these indices is investigated, rather than the complex time-varying and 3-dimensional structure of the beach surface. Although shoreline prediction is the focus of this study, intertidal

beach volumes have been shown to be coherent with shoreline evolution [6, 7, 8] and therefore the approach developed here is expected to be transferable.

Recently, models of 'reduced complexity' [6, 10] have been shown to provide skilful hindcasts of coastal change on both cross-shore [11, 12, 13, 14, 15] and longshore transport dominated [16, 17, 18, 19, 20] coastlines. The simplicity and stability of such models unlocks the exciting potential for much longer-term (months-years-decades) hindcasts and even forecasts of coastal change.

Skilful hindcasting of coastal evolution with known forcing conditions is a necessary precursor to forecasting of future coastal change. Short-term deterministic forecasts with a 5- to 10-day prediction horizon can be achieved with the aid of accurate forecasts of wave forcing derived from physics-based weather models [21]. However, at prediction horizons in excess of this one must fall back on climatological/statistical approaches to forecasting. The latter approach is the subject of the present paper, which develops forecasts up to (and potentially beyond) one year. Climatological approaches can be particularly skilful in predicting weather, when there is a strong, coherent seasonal variability, for example, annual fluctuations in air temperature or wind speed. Although there are some examples of climatological shoreline forecasting (e.g. [22]), this research area is still in its infancy.

In this contribution multiple synthetic wave time series are derived from a pool of measured data and subsequently used to force a Monte Carlo shoreline simulation using a simple equilibrium model. Monte Carlo methods have been implemented for the prediction of shoreline change in the past (e.g. [12, 23, 24]), however the approach taken here is somewhat different. A robust statistical generalised extreme value (GEV) analysis is used to predict the magnitude of shoreline displacement for pre-defined recurrence probabilities. Details of the two field sites with contrasting wave climates and tidal regimes, which are used to test the forecasting methodology are given is section 2. This is followed by an overview of the forecasting methodology in section 3, including a description of the shoreline model, the method of generating multiple synthetic wave records using measured or modelled data and finally the method of generalised extreme value analysis (GEV), which gives shoreline displacements for specified recurrence probabilities. In section 4 the results of this procedure are presented for both the storm and recovery period of two major storms

experienced at two contrasting sites. The finding of this research and future developments are summarised in sections 5.

2. Site Description

Two extensive shoreline datasets and complementary wave measurements at highly contrasting environments (Table 1) are used to provide a rigorous test of a shoreline forecasting methodology. Both environments are energetic, cross-shore transport dominated, swash-aligned coastlines, but each has very different temporal variability in their wave climate and shoreline response. Specifically, the two sites are: Perranporth, with a highly seasonal wave climate, located on the exposed Atlantic west coast of Cornwall in the UK [25] and Narrabeen, with a storm dominated wave climate, located on Sydney's northern beaches on the eastern seaboard of Australia [26], (Figure 1). A summary plot showing the seasonal succession of ensemble-averaged parameters that will be subsequently used to force the shoreline model and the measured shoreline responses for both Perranporth and Narrabeen are shown in Figure 2. The forcing parameters include wave power and dimensionless fall velocity, $\Omega = H_b / \omega T$ [27], where H_b is the breaker height, ω is the fall velocity of the beach sediment and T is the peak wave period.

The Perranporth wave data in Figure 2 is based on a 65-year record of hourly Wave Watch III modelled offshore (73 m depth) significant wave height and period data for the location of the Sevestones Lightship [28] and a complementary time-series of the cross-shore position of the shoreline, extracted from GPS surveys conducted over an 8-year period [29]. The Narrabeen data used here includes a 36-year record of hourly offshore wave statistics, measures at Sydney's wave rider buoy (depth 74 m) and a complementary 8-year time-series of shoreline displacements. For consistency, shorelines at both sites were centred on the mean high-water contour line, which was averaged over a 400 m longshore distance and sampled at monthly time intervals.

2.1 Perranporth, UK

Perranporth, is a 3.5 km long, macrotidal (mean spring tidal range 6.5 m) beach situated on the northern coast of the UK's southwest peninsula (Figure 1a). It is directly exposed to normally incident, energetic and highly seasonal swell waves generated by anticyclones propagating on a general westerly track across the northern Atlantic Ocean. This seasonality in the wave climate is

shown clearly in the monthly-averaged wave power, where energetic, long-period swell waves arriving during the November to January are ≈5.5 times higher than the (June-August) summer months (Figure 2a).

Beach sediments are comprised of quartz sand with average D_{50} of 0.33 mm and a fall velocity of 0.04 m/s [30]. Monthly-averaged dimensionless fall velocities at Perranporth are in the range (4.5-6) indicating intermediate to dissipative beach states which are consistent with observations. The modal classification at Perranporth is low-tide bar and rip according to the classification of Masselink and Short [31]. However, winter periods are often typified by highly dissipative beach states.

The shoreline response at Perranporth (Figure 2e) shows high variance at annual time-scales, with shoreline erosion commonly evolving smoothly over the November to February fraction of the year in response to a succession of erosive storms, rather sharp step-like displacements relating to individual storm events (Figure 2). During this winter storm season the horizontal displacement of the mean high water contour can be very large, exceeding 70 m. Beach recovery begins in late March and proceeds at a much slower rate (≈ 1/4) than the erosion, often persisting until October.

Interannual variability in the wave climate is dominated by the North Atlantic Oscillation index with more positive values being indicative of stronger westerly winds and waves [29], although the direct link with shoreline erosion and morphology remains unsubstantiated [32].

2.2 Narrabeen, Australia

Narrabeen is a microtidal (mean spring tidal range ≈ 1.5 m), 3.5 km long, embayment, situated on Sydney's northern beaches (Figure 1b). The Narrabeen wave climate is dominated by two principle components. The first is a moderate to high energy condition which prevails from the S/SE with a mean period and wave height of T_p ≈10 s and H_s ≈ 1.6 m respectively and is generated by mid-latitude cyclones propagating over the Tasman Sea [33, 34]. The second component are storm events (H_s >3 m) which represent 6% of the observed wave field [35]. Storms vary seasonally, with most storms occurring in winter (39%), fewest storms occurring in summer (12%) and transitional periods observed in autumn (26%) and spring (23%) [34]. Winter storms are

156 characterized by high power waves from a S/SE direction generated by mid-latitude cyclones from
157 the south and east coast low pressure systems. Notice however that the maximum monthly-
158 averaged offshore wave power at Narrabeen is only a third of that observed at Perranporth (Figure
159 2b and c). The summer wave climate is dominated by NE short period waves generated by a local
160 sea breeze [33]. Interannual variability in the Sydney wave climate is influenced by the Southern
161 Oscillation Index, in particular the La Niña phase is associated with an increase in storm frequency
162 and duration with a dominant NE/E direction, whereas El Niño phase is characterized by milder
163 SE/S wave conditions [36, 34].
164
165 Narrabeen is characterised by coarser sand than Perranporth (D_{50}≈0.4 mm), and monthly-mean
166 dimensionless fall velocities (Ω=3.4-3.8) that are indicative of the range of intermediate beach
167 states that are observed, including both welded and detached bar states. Interestingly,
168 dimensionless fall velocities are lowest in the Austral winter even though winter waves are more
169 energetic. This factor relates to the longer wave periods associated with the winter swell.
170
171 The surfzone width at Narrabeen is relatively narrow compared to Perranporth, leading to efficient
172 sediment transport between the beach face and sandbars and more rapid shoreline displacements,
173 which typically proceed at monthly (storm) time-scales. In spite of this rapid shoreline response
174 there is also a significant seasonal signal at Narrabeen, with erosion during the months of April to
175 July and beach recovery predominantly in the subsequent November to March period (Figure 2f).
176 Maximum shoreline displacements at Narrabeen are half (≈ ±20 m) that observed at Perranporth
177 and the seasonal range less than a quarter (≈ ±10 m, Figure 2e and f). Splinter *et al*., [15]
178 characterised the relative seasonal to storm dominance by the ratio of the yearly- and monthly-
179 average standard deviations in dimensional fall-velocity, whereby values significantly greater than
180 1.0 typify highly seasonality. The storm dominance at Narrabeen is again highlighted by the
181 observed value of $\sigma_{\Omega 365}/\sigma_{\Omega 30}$ = 1.07, which is some 13% lower than that observed at Perranporth
182 (1.22). Due to this storm dominance it might be expected that the shoreline dynamics of this Pacific
183 east coast site will be the most challenging to forecast meaningful shoreline responses due to the
184 episodic nature of the storms.
185

2.3 Extreme Storms

In this section, we focus on two notable extreme storm sequences recorded at Perranporth and Narrabeen. At Perranporth the extreme storms in the November-February period of 2013/14 produced the most powerful sequence of waves observed in the past 65-years causing over 70 m of shoreline recession. Masselink *et al*., [37] reported that 22 storms (each >1% exceedance in offshore significant wave height) were observed in this period. At Narrabeen the model will be tested on a powerful sequence of extreme storms recorded during the La Niña year in June 2007, which caused the bulk tanker Pasha Bulker to run aground on a beach north of the site and resulted in over 35 m of shoreline recession at Narrabeen [38], hereafter referred to as the 'Pasha Bulker storm'.

3. Forecasting methodology

This section briefly describes the equilibrium shoreline model that is used to derive the shoreline forecasts. A detailed description of the model is avoided here and instead the Reader is directed to Davidson *et al*., [39] and Splinter *et al*., [15] for a more thorough description and validation of the model. After the brief description of the model, details of the calibration and validation are given. This is followed by a description of the simulation of the synthetic wave forcing parameters that are used to force the shoreline model in a Monte Carlo fashion and form the basis of the generalised extreme value analysis.

3.1 ShoreFore - Model Description

The shoreline change with time is expressed as a function of the incident wave power (P) and the disequilibrium in the dimensionless fall velocity $\Delta\Omega$.

$$\frac{dx}{dt} = c^{\pm} P^{0.5} \Delta\Omega \quad (1)$$

Here c is the response rate coefficient that controls the magnitude of the shoreline response per measure of wave power [m/(W/m)$^{0.5}$]. The response rate parameter takes different values depending on whether the shoreline is eroding or accreting. The sign of the shoreline displacement is controlled by the disequilibrium in the dimensionless fall velocity ($\Delta\Omega$), which is given by:

$$\Delta\Omega = \frac{1}{\sigma}\left(\Omega_{\phi} - \Omega\right) \quad (2)$$

Here Ω is the instantaneous dimensionless fall velocity and Ω_ϕ is a weighted average of the antecedent dimensionless fall velocity by the following weighting function [40].

$$\Omega_\phi = \left[\sum_{i=1}^{2\phi} 10^{-i/\phi}\right]^{-1} \sum_{i=1}^{2\phi} \Omega_i 10^{-i/\phi} \quad (3)$$

and σ is the standard deviation of (Ω_ϕ-Ω), such that ΔΩ has unit standard deviation and primarily controls the sign of the shoreline change. The model predicts erosion when incident waves are steeper than the weighted average (antecedent) conditions and visa-versa for accretion. A strong hysteresis in the shoreline behaviour is implicit in this model, whereby future change is highly dependent on the antecedent forcing conditions. Thus, forecasts of shoreline position are not just a function of the future forcing conditions, they are also strongly influenced by the antecedent conditions. The parameter ϕ is measured in days and controls the decay in the weighting function which has a value of one at the prediction time, decaying to 0.1 and 0.01 at ϕ and 2ϕ days respectively before the prediction time. The value of ϕ effectively controls the frequency of the shoreline response with values $>>10^2$ days producing a dominantly seasonal shoreline response (given some seasonality in the observed wave climate), typical of dissipative beaches, whilst values $<10^2$ days produce a higher frequency storm response, typical of more intermediate beaches [15]. Note that for a given site with consistent grainsize, the variability in the forcing parameters (*P* and Ω) is controlled only by hydrodynamic variables (H_b and *T*). We require synthetic values of these parameters, which reflect the observed seasonal statistics of the wave field, in order to generate the shoreline forecasts.

3.2 Model Calibration

Figure 3 shows the wave power time-series alongside the respective model calibrations and validations for both the Perranporth and Narrabeen data sets. Here the two major storm sequences have been omitted from the model calibration and have been used here to validate the models capacity to hindcast two major storm events, using measured forcing parameters. These storms are the Pasha Bulker storm sequence in June 2007 at Narrabeen and the extraordinary storm sequence which struck the exposed energetic coastlines of the north Atlantic during the winter of 2013/14. These storms will be used later to test the forecasting method and the true wave forcing for these

periods will remain unseen for both the model calibration and the later forecasts in order to provide a rigorous test of the methodology.

As shown in Figure 3, model hindcasts are highly skilful at matching observations for both calibration (r = 0.92 Perranporth; r = 0.87 Narrabeen) and validation (r = 0.98 Perranporth; r = 0.89 Narrabeen) subsets of the data at both sites. It is noted that the model optimised ϕ values for both sites are 15 days for Narrabeen, typical values for a storm-dominated intermediate beach, in contrast to 450 days for Perranporth, in keeping with this contrasting site exhibiting a seasonally-dominated dissipative beach.

3.4 Generating Synthetic Time-series

A quasi-Monte Carlo simulation method is adopted here for forecasting the shoreline climatology. A similar method of shoreline forecasting was suggested by Davidson *et al*., [12], who implemented the method of Borgman and Scheffner [41] to generate synthetic wave series based on the monthly, statistical variability in wave height, period and direction in the measured wave field. This contribution moves on from this work by implementing a different method of synthetic wave generation, and the application of a more sophisticated GEV analysis of the model output.

Generation of synthetic waves involves the assembly of a large number of forcing time-series, used later to drive the shoreline model. The key forcing parameters for the ShoreFor model are wave power (P) and dimensionless fall velocity (Ω) time-series. These synthetic series must reflect the measured or modelled statistical properties for the prediction site. Each of the resulting forcing series are used to generate a shoreline forecast using the calibrated ShoreFor model detailed in the previous section. Typically, N=10^3 synthetic time-series are generated for the Monte Carlo simulations. The number of simulations is easily extended given the computational efficiency of the method, but 10^3 estimates was found to provide stable, consistent forecasts. A rigorous statistical GEV analysis of the resulting shoreline data is then used to compute the magnitude of both shoreline accretion and erosion corresponding to specified recurrence probabilities.

In the present contribution, we restrict our forecast horizon to one year. This is done because a meaningful multiyear forecast requires additional knowledge of the likely inter-annual variability.

The forecasting methodology used here does not include this, although work is currently in progress to extend the predictions in this direction.

A pool of either modelled (i.e. Perranporth), measured or a combination of these (i.e. Narrabeen) wave data is used to generate new times series of both P and Ω. This is done by building multiple, annual time-series of P and Ω on a month-by-month basis, by selecting an equivalent month of data from the available wave data corresponding to a randomly selected year. As each month is incremented a different random year is selected each time. This method is simple but very effective in conserving the monthly evolution of the statistical properties in the observed wave field, as well as accurately preserving the sequencing of waves. The size of the wave data pool for Perranporth and Narrabeen examples were 63 years and 36 respectively. The impact of the size of the data pool on predictions is examined later in this section.

In order for the test to be rigorous, the data pool used to generate the synthetic time-series must exclude the forecasting period, even if the data are in fact known (i.e. hindcast). The data pool must also be consistent with the wave data used to calibrate and validate the model (same source or statistically similar).

Future modifications of the wave climate, due to climate change for example, are not included in these tests; a reasonable assumption for an annual time-scale of the forecasts presented here. It is assumed that the wave data 2ϕ-years prior to the prediction date (t_0) is known (equivalent to the maximum width of filter function window, equation 3) in order to evaluate the appropriate antecedent conditions, (Figure 4). Each of the new synthetic time-series are concatenated on the end of these 2ϕ-years of observed data (Figure 4). It is the combination of the known antecedent conditions and unknown future wave conditions which will determine the nature of the forecast.

Figure 5 shows an example of the resulting 10^3 Monte Carlo shoreline predictions corresponding to the synthetic forcing series. Notice that these simulations were started on the 1st October 2013, just prior to the extreme storms at Perranporth. Thus, the distribution shows an initial tendency for erosion (negative mean displacements), with recovery beginning in April and returning to near zero mean displacement by the end of the year. Notice also the spread in shoreline predictions for

each month of the year, a distribution that will be characterised by the Generalised Extreme Value (GEV) analysis detailed in the next section.

3.5 Generalised Extreme Value (GEV) Analysis

Here we extract from the shoreline prediction matrix the independent, extreme values of shoreline position (for both erosion and accretion) for each simulation, corresponding to a regular time interval in the forecasts. Care is taken to use only unique shoreline series as the random generation method for the forcing series used here can potentially produce identical forcing and therefore replica shorelines. Typically, monthly intervals are used here, although this window duration can easily be varied. These monthly extremes from each of 10^3 simulations are plotted as histogram and a GEV probability distribution function (PDF) is fitted to the data. The GEV analysis used here focusses on accurately fitting the tails (extremes) of the distribution (rather than the peaks) and allows the data to instruct which of three distribution options is most appropriate to the observations [42]. These options are controlled by a shape function k which dictates the decay structure at the limits of the distribution. Here an exponential decay is selected for k=0 (e.g., normal, Gumbel, [43]), a polynomial for k>0 (e.g. student's t-test, Fisher and Tippett, [44]), or k<0 if the extreme is finite (e.g. Weibull, [45]). The form of the extreme value distribution PDF is:

$$y = f(x|k,\mu,\sigma) = \left(\frac{1}{\sigma}\right) exp\left(-exp\left(-\frac{(x-\mu)}{\sigma}\right) - \frac{(x-\mu)}{\sigma}\right) \quad \text{for } k=0 \qquad (4)$$

or

$$y = f(x|k,\mu,\sigma) = \left(\frac{1}{\sigma}\right) exp\left(-\left(1+k\frac{(x-\mu)}{\sigma}\right)^{-\frac{1}{k}}\right)\left(1+k\frac{(x-\mu)}{\sigma}\right)^{-1-\frac{1}{k}} \quad \text{for } k\neq 0 \qquad (5)$$

Here μ is the mean and σ is the standard deviation. Conveniently, users of Matlab will find that the statistical toolbox has a useful function for achieving the optimised fit to observations. The methodology was found to be most successful and very robust when fitting to the negative of the observed shoreline distribution (i.e. negative accretion and positive erosion) and then accounting for the change in sign later (reverting to the positive accretion and negative erosion convention) in the subsequent analysis and figures.

The classification of appropriate thresholds in order to define storms or events is non-trivial and usually effects the ultimate prediction of return magnitudes and periods of the series being analysed [46]. Additionally, wave and shoreline time-series are fundamentally different, for example extreme storms may have annual occurrences of $O(10^1)$, occurring in multiple months, whereas shoreline series typically have single annual maxima/minima occurring in just one month of the year. This fact means that it is potentially erroneous to borrow established thresholding techniques which have been established for wave data and apply them directly to morphological time-series.

As is the case with storm-wave thresholds, magnitude-based thresholds for shoreline displacement would necessarily differ from site-to-site, depending on the size of the observed shoreline variability. Here we seek a common methodology that will be equally applicable to all sites, irrespective of the size of the observed shoreline variability. For this reason, a probability of occurrence threshold has been applied to the shoreline forecasts. Notice also, that unlike wave forecasts, which seek to apply only a storm threshold to isolate the highest waves, a bi-directional threshold is sort here to separate normal from high erosion and accretion events. Since we are dealing here with both erosion and accretion, it is also inappropriate to define shoreline displacements above threshold as storms, therefore we will refer to shoreline displacements which exceed threshold value as *events* in the following text.

This methodology defines three erosion and three accretion bands using the cumulative GEV PDF function, which has been fitted to the model forecast data. Erosion and accretional bands are defined by *Pr* and (1 - *Pr*) respectively, where *Pr* is the probability threshold for the band. Here we characterise the intensity of the cross-shore shoreline displacements with a colour-coded traffic light system. These three bands are normal (green), high (amber) and extreme (red) and described in detail below:

1) Normal (green): This band includes predictions which typify annual shoreline displacements. Predictions in this band are not characterised as events and have recurrence probabilities constrained by the *event* probability ($Pr_{threshold}$), whereby, the erosion/accretion limits of this band are: $Pr_{threshold}$ < Normal band limits < 1-$Pr_{threshold}$.

2) High (amber): These are predicted shoreline displacements which are classified as events having recurrence probabilities lying outside of the green band but constrained within: $Pr_{threshold}/100$ < High band limits < 1 - ($Pr_{threshold}/100$). Thus, the outer limits of this band typify the probability of a 1/100 recurrence event.
3) Extreme (red): This band defines extreme *events* with probabilities outside of the high band but encompassing the extremes of the predictions. In these simulations, this condition was satisfied by setting the erosion/accretion limits at: $Pr_{threshold}/10^7$ < Extreme band limits < 1 – ($Pr_{threshold}/10^7$). Where the factor of 10^7 is an arbitrarily selected high value.

The erosion and accretional bands are separated by the mean (central tendency, μ) of the shoreline forecasts, which is also a bi-product of the GEV PDF fit to data (equations 4 and 5). Much like any other extreme value analysis the traffic light system used here is sensitive to the threshold value ($Pr_{threshold}$). Here we have elected to use a recurrence probability rather than an amplitude threshold on the grounds that this methodology should be less site specific. Nonetheless, the methodology is sensitive to the value of event threshold selected. We examine this sensitivity in the results section by varying the threshold between one month per year ($Pr_{threshold}$=1/12) and one day per year ($Pr_{threshold}$=1/365).

The inverse of the fitted GEV PDF is used to return shoreline positions corresponding to the pre-mentioned probability values and define the limits of these three bands. Example histograms for Monte Carlo shoreline forecasts, extracted from the data in Figure 5 for the time intervals marked a-f are shown in Figure 6 (also labelled a-f). The traffic light coding and PDF fits to the data are also shown in these figures. Notice how well the GEV PDFs fit the tails of the distributions (amber and red bands). Encouragingly, the pre-mention bands encapsulate both the extremes of the data and the range shoreline displacements categorised as normal correlate well with the observed time-series.

3.6 Sensitivity of model forecasts to the duration of the wave pool

Figure 7 shows an example predictions for the severe 2013/14 storms observed at Perranporth, UK. The GEV PDF and traffic light system have been presented here as a background for the observed data. Note that the probability threshold defining an event $Pr_{threshold}$ has been set to 1/12

in these examples. This is annual forecast starting at the beginning of October 2013 and running through the extreme storm sequence and subsequent recovery period. Also presented in Figure 7, is the sensitivity of the forecasts to the total duration of the wave data pool used to generate the synthetic forcing for the model. Here we progressively reduce the data pool at Perranporth from 60-years to just 10-years prior to the sample date. It can be seen from these plots that in all cases the observations fall within the predicted limits of the extreme (red) band.

The forecast which utilised 60-years of wave data (Figure 7a), shows that the shoreline response to the winter storms is on the boundary between the high-range and extreme range with an expected event recurrence probability close to 1/100, for this prediction starting 2-months prior to main shoreline recession. This classification remains consistent within the uncertainty of the data, for wave pool sizes of at least 20-years but changes to an extreme classification (red) for a wave pool size of just 10 years. Based on this and other tests (not shown) the authors suggest that the wave pool size should exceed 15-years in order to achieve consistent forecast classifications, although a firm conclusion on this point will probably require experimentation at additional sites.

4. Results

4.1 Perranporth, UK

Figure 8 shows both the forecast and measured shoreline impact and subsequent recovery of the 2013/14 winter storms at Perranporth ($Pr_{threshold}$=1/12). In order to capture a complete season of recovery-erosion-recovery, forecasts start 7-months prior to the main storm impacts on the 1st May 2013 during the beach recovery phase and proceeds with start times (t_0) incrementing in two-month intervals through the storm and up to the start of the post-storm recovery. In doing so we are able to answer two key coastal management questions, namely: Can we predict the likely impact of the next extreme storm sequence? And, can we forecast beach recovery after the impacts of an extreme storm sequence?

Figure 8a shows the shoreline forecast during the recovery period, prior to the main storm. The forecast predicts a narrow range of potential shoreline projections over the coming six-months. It is not until the onset of the winter storms, when there is a tendency for erosion that the predicted range in shoreline responses widens significantly. Inspection of the measured data in this plot

shows that shoreline recovery in this example (Figure 8) is slow initially, remaining in the lower-amber range during the period leading up to the storms, but reaching the low-normal (green) range by December 2013.

Pre-storm shoreline positions were at the shoreward-extreme of the normal range prior to the storms (i.e. somewhat eroded for the time of year). In all cases the data are effectively captured within the prediction band and the range of the predictions is not so excessive as to be of limited value. This example (Figure 8a) shows that for this seasonally dominated site, shoreline recovery is indeed predictable and can be forecast.

The classification of the observed 2013/14 storm impact (see arrow in Figure 8a), starting 11 months before the maximum observed erosion is extreme (red). This rating has an *event* return probability of less than 1/100. This extreme (red) classification of the storm reduces to the outer limit of the high (amber) band, seven months prior to the maximum storm erosion t_0 = 1st September 2013 (Figure 8c). This is likely due to the fact that the beach levels were already uncharacteristically low for the time of year, just prior to the main storm sequence. This classification then remains consistent right up to the start of the main storm sequence starting in November 2013 (Figure 8d). These results (and threshold selection, $Pr_{threshold}$=1/12), suggest that the Perranporth storm sequence of 2013/14 had an event return probability of ≈ 1/100. This classification even remains consistent through the storm (Figure 8e).

The post extreme-storm recovery is predicted after the 2013-14 storms, starting t_0 = 1st March 2014 in Figure 8f. It can be seen in this second recovery example, that once again, the forecast is tight and accurate. Unlike the pre-storm recovery (Figure 8a), the post recovery is much more rapid, proceeding in the upper-amber range. This was somewhat unexpected as the offshore survey data (not included here) showed that the eroded beach sand had been moved to an offshore bar, located 1 km offshore of the high-tide shoreline position. This extreme translation of sand does not seem to have stunted beach recovery at all. Notice however, that there is quite a bit of uncertainty in the measurements, represented by the error bars in the data during this recovery phase as the beach gets more 3-dimensional in the longshore direction as the sand moves from the offshore sandbar towards beach. Again, Figure 8f supports the notion that beach recovery is indeed predictable at

this site. Notice also that the methodology used here may forecast different outcomes for the same month in different years, due to importance and potentially different antecedent hydrodynamic conditions.

4.2 Narrabeen, Australia

Perhaps a more challenging test for this forecasting methodology is application to a distinctly storm dominated wave climate, with a weaker seasonal signal, where shoreline responses are more rapid. The Narrabeen dataset provides the opportunity to do this. Like the previous Perranporth example, Figure 9a starts during the natural recovery-phase on the 1st October 2006, prior to the Pasha Bulker storm sequence. An identical methodology to that used in the previous example at Perranporth has been applied here to an extreme storm sequence at Narrabeen ($Pr_{threshold} = 1/12$).

It can be seen that the forecast for Narrabeen still provides a useful estimate of shoreline recovery, even in this storm dominated environment (Figure 9a). Comparison with the measured data shows that unlike Perranporth the recovery At Narrabeen prior to the storm is high, lying entirely within the upper end of the normal range (upper-green/amber boundary). This healthy recovery led to a healthy shoreline accretion prior to the inception of the Pasha Bulker storm sequence.

Notice also that the maximum storm erosion, indicated by the arrow, is in all of the pre-storm forecasts (Figures 9a-e), consistently on the erosional amber-red boundary, indicating that shoreline displacement due to the Pasha Bulker storm sequence, like the Perranporth example, has an event probability of ≈1/100. Interestingly, shoreline positions and beach volumes along the New South Wales coastline were not observed to have eroded excessively and certainly would have not been at 1/100 year low after this storm sequence. It is important to make two important points here. Firstly, this methodology is characterising shoreline displacement, rather than absolute shoreline position. Whilst these two measures are similar, large erosion events should correlate with an eroded shoreline, they are not the same thing. In this example, the pre-storm shoreline was quite strongly pro-graded, thus, in spite of considerable storm erosion, the post-storm shoreline was not excessively eroded. The second point to make is that classifications used here (normal, high and extreme) will vary with the somewhat subjective choice of the *event* threshold ($Pr_{threshold}$). This latter point is explored in the next section.

Shoreline recovery after the Pasha Bulker storm is forecasted in Figure 9f. Like the post storm Perranporth example, beach recovery is well forecasted at Narrabeen and is rapid, skirting both the amber (high) red (extreme) intersection.

Sensitivity to the event threshold ($Pr_{threshold}$)

Most extreme value analysis methods are sensitive to the threshold which defines an event. In the previous examples, we have avoided a site-specific amplitude threshold, instead defining a probability of occurrence threshold of 1 month in 1 year ($Pr_{threshold}$ =1/12) to define a shoreline displacement *events* which are likely to be outside the typical annual range. This forms the basis of the traffic light characterisation presented here with outer limit of the high band limited to 1/100 event displacement (Pr =1/1200). Although, the event threshold has been intelligently selected, based on the observation that shoreline time-series reach their minimum and maximum values during just one month of the year, this value is still somewhat subjective.

In order to investigate the sensitivity to the event threshold probability, in figure 10 and 11 we follow an identical methodology to that used to create figures 8 and 9 respectively, but have adjusted the event probability threshold from the reasonable maximum value (1/12) to the likely minimum extreme, 1 day in 1 year ($Pr_{threshold}$ =1/365). Inspection figures 10 and 11 shows that the main impact of reducing the event threshold is to broaden the green (normal) band of the traffic light system with at the expense of the amber and red regions. Because of the shape of the P.D.F functions, the limits of the high and extreme bands (amber and red) are only displaced outward a relatively small amount. The resulting patterns are very similar but the characterisation of the shoreline displacements in figures 10 and 11 are generally downgraded away from the extreme classification and towards the normal band. It is not clear from the analysis exactly what the best threshold setting is, application of the methodology to more storms and more sites will be required in order to establish this. However, this test does serve to illustrate the sensitivity of the classification (normal, high, extreme) to the threshold value.

5. Concluding Remarks

A new methodology for forecasting shoreline displacement has been detailed in this contribution. The methodology includes: generating multiple forcing time-series based on measured or modelled wave data, the implementation of an established shoreline model [39] to drive a Monte Carlo forecast of shoreline behaviour and characterising these shoreline responses with a generalised extreme value (GEV) analysis. Results presented here indicate that it is indeed possible, at least on these exposed, swash-aligned sites, to provide genuine forecasts of the limits of:

a) Shoreline recession due to the impact of a storm sequence.
b) Shoreline recovery after the passage of an extreme storm erosion events.

The methodology provides a probabilistic forecast (P.D.F.) of shoreline displacements, up to a year in advance of the prediction start date and provided a simplistic 'traffic light' classification based on the recurrence probability of an event. Shoreline forecasts are classified as normal (likely to be observed in a typical year), high (*events* outside the typical annual recurrence probability) and extreme (events outside the 1/100 *event*-recurrence probability).

Although the methodology has been tested on time-series of high-water shoreline displacement, it could easily be transferred to the prediction of other definitions of the shoreline position or indeed intertidal beach volumes. Here we use an established shoreline model, ShoreFor [39], but acknowledge that the same methodology could be equally well implemented with other fast and robust models of this genre. The present model is restricted to coasts dominated by cross-shore sediment transport, but other modelling approaches could be combined with this general forecasting methodology, including one-line models, in order to overcome these limitations.

In both applications presented here the models showed highly skilful hindcasts. This is an essential pre-requisite of this forecasting approach. Poor model hindcasts are likely to lead to unreliable forecasts. Here we recommend the model-data calibration coefficients (r) (comparisons between observations and model results) exceed 0.8 for accurate forecasts. Weaker correlations could lead to forecasts that under-predict the magnitude of the shoreline response.

This contribution used measured shoreline data to calibrate the shoreline model. However, the availability of shoreline data is not necessarily a limit to application of this particular model.

548 Splinter *et al*., [15] showed that ShoreFor model free parameters can be estimated using easily
549 available environmental parameters including wave climate and sediment properties.
550
551 A provisional sensitivity analysis shows that the minimum size of the pool of wave data required
552 to produce accurate and consistent forecasts of shoreline response is approximately 15-years,
553 although it is recommended that all the available data are used. In the simulations used here we
554 have implemented forecasts with both modelled (Perranporth) and a mixture of
555 measured/modelled (Narrabeen) wave data, both provided good forecasts of shoreline behaviour.
556 Since the use of commonly available modelled wave data seems to provide robust shoreline
557 predictions, the application of this methodology could potentially be quite widely used to the
558 prediction of extreme shoreline erosion and subsequent beach recovery.
559
560 The forecasts produce accurate representations of the observed shoreline behaviour. The
561 characterisation of the shoreline behaviour (normal, high or extreme) is sensitive to the event
562 probably threshold. Although the precise choice of event threshold remains somewhat ambiguous,
563 provisional results suggest that the most appropriate descriptions of shoreline displacements were
564 achieved by setting event recurrence threshold in the region $Pr_{\text{threshold}} \approx 1/365$ to 1/12. More
565 widespread application of the methodology to different environments will be required in order to
566 converge on the most appropriate event threshold.
567
568 Recent studies indicate that climatic indices can be skilfully predicted a year in advance [46]. The
569 fact that climate indexes (e.g. NAO and ENSO) have been linked to storminess and shoreline
570 change (e.g. Robinet et al., 2016), indicates that it may be possible to make more accurate
571 predictions for the forthcoming year and perhaps beyond, if the synthetic waves used to force the
572 shoreline predictions were based only on past wave data with climate indexes similar to those
573 projected for the forecasting period.
574

575 ## 6. References

576 [1] H.J. De Vriend, J., Zyserman, J., Nicholson, J. A. Roelvink, P. Pechon, and H.N. Southgate.
577 Medium-term 2DH coastal area modelling, *Coastal Engineering*, **21**, (1993), 193–225,
578 doi:10.1016/0378-3839(93)90050-I.

[2] J.A. Roelvink, J. A., & I. Broker. Cross-shore profile models, *Coastal Engineering*, **21**, (1993), 163–191, doi:10.1016/0378-3839(93)90049-E.

[3] L.C. Van Rijn, D.J.R. Walstra, B. Grasmeijer, J. Sutherland, S. Pan, & J. P. Sierra. The predictability of cross-shore bed evolution of sandy beaches at the time scale of storms and seasons using processbased profile models, Coastal Eng., **47**, (2003), 295–325, doi:10.1016/S03783839(02)00120-5

[4] M.A. Davidson, M. Van Koningsveld, A. de Kruif, J. Rawson, R. Holman, A. Lamberti, R. Medina, A. Kroon, and S. Aarninkhof. The CoastView project: Developing video-derived coastal state indicators in support of coastal zone management, *Coastal Engineering*, **54** (6–7), (2007), 463–475, doi:10.1016/j.coastaleng.2007.01.007.

[5] A. Kroon, M.A. Davidson, S.G.J. Aarninkhof, R. Archetti, C. Armaroli, M. Gonzalez, S. Medri, A. Osorio, T. Aagaard, R.A. Holman, R. Spanhoff. Application of remote sensing video systems to coastline management problems, *Coastal Engineering*, **54**(6–7), (2007), 493–505, doi:10.1016/j.coastaleng.2007.01.004.

[6] A.S. Farris and J.H. List. Shoreline as a proxy for subaerial beach volume change. *Journal of Coastal Research* **23**(3), (2007), 740-748.

[7] M.D. Harley, I.L. Turner, A.D. Short & R. Ranasinghe. Assessment and integration of conventional, RTK-GPS and image-derived beach survey methods for daily to decadal coastal monitoring. *Coastal Engineering* **58(2)**, (2011), 194-205

[8] A. Robinet, B. Castelle, D. Idier, G. Le Cozannet, M. Deque & E. Charles. Statistical modelling of Interannual shoreline change driven by North Atlantic climate variability spanning 2000-2014 in the Bay of Biscay. Geo-Mar. Lett. DOI 10.1007/s00367-016-0460-8. (2016).

[9] J.R. French, A. Payo, A.B. Murray, J. Orford, M. Eliot & P. Cowell. Appropriate complexity for the prediction of coastal and estuarine geomorphic behaviour at decadal to centennial scales. *Geomorphology.* DOI: 10.1016/j.geomorph.2015.10.005, (2016).

[10] A.B. Murray. Reducing model complexity for explanation and prediction. *Geomorphology*, **90**(3), (2007), 178-191.

[11] M.A. Davidson, I.L. Turner. A behavioural template beach profile model for predicting seasonal to inter-annual shoreline evolution. *Journal of Geophysical Research*, **114**, (2009), 1–21.

610 [12] M.A. Davidson, R. P. Lewis, and I. L. Turner. Forecasting seasonal to multi-year shoreline
611 change, Coastal Eng., **57**, (2010), 620–629, doi:10.1016/j.coastaleng.2010.02.001.
612 [13] M.L. Yates, R.T. Guza & W.C. O'Reilly. Equilibrium shoreline response: Observations and
613 modeling, J. Geophys. Res., **114**, C09014, doi:10.1029/2009JC005359, (2009).
614 [14] M.L. Yates, R.T. Guza, W.C. O'Reilly, J.E. Hansen & P.L. Barnard. Equilibrium shoreline
615 response of a high wave energy beach, J. Geophys. Res., **116**, C04014,
616 doi:10.1029/2010JC006681. (2011).
617 [15] K.D. Splinter, I.L. Turner, M.A. Davidson, P. Barnard, B. Castelle & J. Oltman-Shay. A
618 generalized equilibrium model for predicting daily to inter-annual shoreline response.
619 *Journal of Geophysical Research: Earth Surface*, (2014), 1936–1958.
620 [16] H. Hanson & N. Kraus. Generalized model for simulating shoreline change, Report 1,
621 Technical Reference, Tech. Rep., U. S. Army Engineer Waterways Experiment Station;
622 Coastal Engineering Research Center (U. S.); United States. Army. Corps of Engineers,
623 (1989).
624 [17] H. Hanson. GENESIS: a generalized shoreline change model. *Journal of Coastal Research* **5**
625 (1), (1989), 1–27.
626 [18] I. Turki, R. Medina, M. Gonzalez & G. Coco. Natural variability of shoreline position:
627 Observations at three pocket beaches. *Marine Geology* **338**, (2013), 76–89.
628 http://dx.doi.org/10.1016/j.margeo.2012.10.007
629 [19] A.D. Ashton, A.B. Murray & O. Arnoult. Formation of coastline features by large-scale
630 instabilities induced by high-angle waves. *Nature*, **414**(6861), (2001). 296-300.
631 [20] A.D. Ashton & A.B. Murray. High-angle wave instability and emergent shoreline shapes: 1.
632 Modeling of sand waves, flying spits, and capes. *Journal of Geophysical Research: Earth*
633 *Surface* (2003–2012), **111**(F4), (2006).
634 [21] F. Baart, M. van Ormondt, J.S.M., van Thiel de Vries, and M. van Koningsveld.
635 Morphological impact of a storm can be predicted three days ahead. Computers &
636 Geosciences, **90, (B)**, (2016), 17–23.
637 [22] N.L. Frazer, A.S. Genz and C.H. Fletcher. Toward Parsimony in Shoreline Change Prediction
638 (I): Basis Function Methods. Journal of Coastal Research: **25**(2), (2009), 366 – 379.

639 [23] P. Ruggiero, J. List, D. Hanes & J. Eshleman. Probabilistic Shoreline Change Modelling.
640 Proc. 30th International Conference on Coastal Engineering, September 2006, San Diego,
641 CA. (2006).
642 [24] D. E. Reeve, A. Pedrozo-Acuña, M. Spivack. Beach memory and ensemble prediction of
643 shoreline evolution near a groyne. Coastal Engineering, **86**, April 2014, (2014), 77–87.
644 [25] M.A. Davidson, D.A. Huntley, R.A. Holman & K. George. The evaluation of large-scale
645 (km) intertidal beach morphology on a macrotidal beach using video images. Proceedings
646 Coastal Dynamics '97. ASCE, (1997), 385-394.
647 [26] I.L. Turner, M.D. Harley, A.D. Short, J.A. Simmons, M.A. Bracs, M.S. Phillips & K.D.
648 Splinter. A multi-decade dataset of monthly beach profile surveys and inshore wave
649 forcing at Narrabeen, Australia. Scientific Data **3**, Article number: 160024.
650 doi:10.1038/sdata.2016.24, (2016).
651 [27] M.R. Gourlay. Beach and dune erosion tests. Rep. M935/M936. Delft Hydraulics Laboratory,
652 Delft, Netherlands. (1968).
653 [28] G. Dodet, X. Bertin, & R. Taborda. Wave climate variability in the North-East Atlantic Ocean
654 over the last six decades. *Ocean Modelling* **31**, (2010), 120–131.
655 [29] G. Masselink, M. Austin, T. Scott, T. Poate & P. Russell. Role of wave forcing, storms and
656 NAI in outer bar dynamics on a high energy, macro-tidal beach. *Geomorphology*, **226**,
657 (2014), 76-93.
658 [30] S. Prodger, P.E. Russell, M.A. Davidson & T. Scott. Understanding and predicting the
659 temporal variability of sediment grain size characteristics on high-energy beaches.
660 *Marine Geology* Volume **376**, 1 June 2016, (2015), 109–117.
661 [31] G. Masselink & A.D. Short. The effect of tidal range on intertidal beach morphology: a
662 conceptual model. *J. Coastal Research* **9**, (1993), 785-800.
663 [32] T. Thomas, M.R. Phillips, A.T. Williams & R.E. Jenkins. Medium-scale behaviour of adjacent
664 embayed beaches: influence of low energy external forcing. *Applied Geography* **32**,
665 (2012), 265-280.
666 [33] A.D. Short & N.L. Trenaman. Wave climate of the Sydney region, an energetic and highly
667 variable ocean wave regime. *Australian Journal of Marine and Freshwater Research* **43**,
668 (1992), 765–791.

669 [34] M.D. Harley, I.L. Turner, A.D. Short & R. Ranasinghe. Interannual variability and controls
670 of the Sydney wave climate. *International Journal of Climatology*, **1335**, (2010), 1322–
671 1335
672 [35] D. Lord & M. Kulmar. The 1974 storms revisited: 25-years experience in ocean wave
673 measurement along the south-east Australian coast. In *Proceedings, International*
674 *Coastal Engineering Conference*, Sydney, (2000), 559–572.
675 [36] R. Ranasinghe, R. Mcloughlin, A.D. Short & G. Symonds. The Southern Oscillation Index,
676 wave climate , and beach rotation. *Marine Geology*, **204**, (2004), 2–7.
677 [37] G. Masselink, T. Scott, T. Poate, P. Russell, M. Davidson & D. Conley. The extreme
678 2013/2014 winter storms: hydrodynamic forcing and coastal response along the
679 southwest coast of England. *Earth Surface Processes and Landforms*. DOI:
680 10.1002/esp.3836. (2014).
681 [38] M.D. Harley, I.L. Turner, K. D. Splinter, M.S. Phillips & J.A. Simmons. Beach response to
682 Australian East Coast Lows: a comparison between the 2007 and 2015 events, Narrabeen-
683 Collaroy Beach. Journal of Coastal Research. SI **75**, (2016), 388-392
684 [39] M.A. Davidson, K.D. Splinter & I.L. Turner. A simple equilibrium model for predicting
685 shoreline change. *Coastal Engineering*, **73**, (2013), 191–202. Available at:
686 http://www.sciencedirect.com/science/article/pii/S0378383912001676
687 [40] L.D. Wright, A.D. Short & M.O. Green. Short-term changes in the morphodynamic states of
688 beaches and surfzones: an empirical predictive model. *Marine Geology* **62**, (1985), 339-
689 364.
690 [41] L.E. Borgman, N.W. Scheffner. Simulation of Time Sequences of Wave Height, Period, and
691 Direction. Technical Report DRP-91-2,54. US Army Corps of Engineers, Washington,
692 (1991).
693 [42] S. Kotz, & S. Nadarajah. Extreme Value Distributions: Theory and Applications. London:
694 Imperial College Press. (2000).
695 [43] E.J. Gumbel. "Statistics of Extremes." Columbia University Press, New York. (1958).
696 [44] R.A. Fisher & L.H.C. Tippett. Limiting forms of the frequency distribution of the largest and
697 smallest member of a sample." Proc. Cambridge Philosophical Society 24, (1928), 180-
698 190.

[45] W. Weibull. A statistical distribution function of wide applicability, *J. Appl. Mech.-Trans.* ASME **18(3)**, (1951), 293-297.

[46] Z. Liu & H. Burcharth. Encounter Probability of Individual Wave Height. Coastal Engineering 1998, (1999), 1027-1038. doi: 10.1061/9780784404119.076

[47] N. Dunstone, D. Smith, A. Scaife, L. Hermanson, R. Eade, N. Robinson, M. Andrews & J. Knight. Skilful predictions of the winter North Atlantic Oscillation one year ahead. Nature Geoscience 9, (2016), 809–814 doi:10.1038/ngeo2824.

Acknowledgements

A special thanks to Gerd Masselink, Paul Russel, Tim Scott, Tim Poate, Martin Austin, Kit Stokes, Peter Ganderton and all others who contributed to the Perranporth data set included in this paper. This research was funded by the Australian Research Council Discovery Grant DP150101339. Mark Davidson would like to extend a special thanks to Water Research Laboratory, School of Civil and Environmental Engineering, UNSW Sydney for additional funding and hosting his visits to work with the Australian team and to all of the staff at the Water Resources Laboratory for making this such a pleasant and productive sabbatical.

List of Figures

729 Figure 4. An example of the synthetic forcing time-series (wave power [top] and dimensionless
730 fall velocity [bottom]) used to drive the shoreline forecast. This is an annual forecast starting
731 on the 1st October 2013 (dotted vertical line). Noticed that each record starts with 6-years of
732 observed antecedent measurements to which 1000 different, year-long, synthetic series are
733 appended.
734 Figure 5 This figure shows the 1000 resulting shoreline estimates generated from applying the
735 forcing series in figure 4 to the ShoreFor model. The ensemble-mean tendency is shown by the
736 solid black line, illustrating the seasonal trend in shoreline erosion and accretion. The letters
737 and arrow represent the shoreline data shown in the figures 6 a to f. ($Pr_{threshold}$=1/12)
738 Figure 6. Histograms of the shoreline data for different months after the start of the forecast t_0 =1
739 October 2013. All shoreline positions are relative to the starting location at t_0. Also shown is
740 the extreme value analysis probability density function fitted to the data (solid black line). The
741 traffic light system represents the normal (green), high (amber) and extreme range (red).
742 ($Pr_{threshold}$=1/12)
743 Figure 7. Sensitivity analysis on the duration of the wave pool used to generate the synthetic wave
744 time-series. Data are shown with error bars representing +/- two standard deviations in the 400m
745 longshore shoreline contour, which have need averaged to give the shoreline estimates [open
746 circles]. Notice that the classification of the storm remains unchanged until the wave pool is
747 decimated to 10-years. ($Pr_{threshold}$=1/12)
748 Figure 8: Six forecasts of shoreline displacements for Perranporth Beach, UK (seasonally
749 dominated system), starting during the pre-storm recovery period in May and progressing in 2-
750 mothly intervals until the post-storm recovery period in March 2014. The arrow indicates the
751 maximum shoreline recession due to the storm in each case. ($Pr_{threshold}$=1/12)
752 Figure 9 Forecasted shoreline response for Narrabeen, Australia (storm dominated system).
753 Forecasts start with t_0 at the pre-storm recovery phase in October 2006 and progress at two-
754 monthly intervals through the main storm sequence in June 2007 and to the post-storm recovery
755 starting in August 2007. ($Pr_{threshold}$=1/12)
756 Figure 10. Similar Perranporth example plot to Figure 8 with a modified event probability
757 threshold of $Pr_{threshold}$=1/365.
758 Figure 11. Similar Narrabeen example plot to Figure 9 with a modified event probability threshold
759 of $Pr_{threshold}$=1/365.

760

761 **List of Tables**

762 Table 1. Comparative data/site characteristics for Perranporth and Narrabeen, including annual
763 average deep-water wave characteristics and sediment properties. $\sigma_{\Omega 360}/\sigma_{\Omega 30}$ is a seasonality
764 index (Splinter *et al*., [15]) describing the ratio of the average annual to monthly standard
765 deviation in dimensionless fall velocity, higher values indicating increased seasonality. Notice
766 that seasonality at Perranporth is some 20% higher than Narrabeen and that dimensionless fall
767 velocities are double a Perranporth indicating more dissipative beach states.

Site	H_s [m]	T_p [m]	Ω	D_{50} [mm]	ω [m/s]	$\sigma_{\Omega 360}/\sigma_{\Omega 30}$	Survey Method (interval)	Wave data [Yrs]	Wave Measurement (type)	Depth
Perranporth	1.98	8.3	5.30	0.33	0.04	1.22	Survey (monthly)	63	Sevenstones (modelled)	73
Narrabeen	1.62	9.6	3.67	0.40	0.05	1.07	Video (weekly)	36	Sydney (measured)	74

Table 1. Comparative data/site characteristics for Perranporth and Narrabeen, including annual average deep-water wave characteristics and sediment properties. $\sigma_{\Omega 360}/\sigma_{\Omega 30}$ is a seasonality index (Splinter et al., 2014) describing the ratio of the average annual to monthly standard deviation in dimensionless fall velocity, higher values indicating increased seasonality. Notice that seasonality at Perranporth is some 20% higher than Narrabeen and that dimensionless fall velocities are double a Perranporth indicating more dissipative beach states.

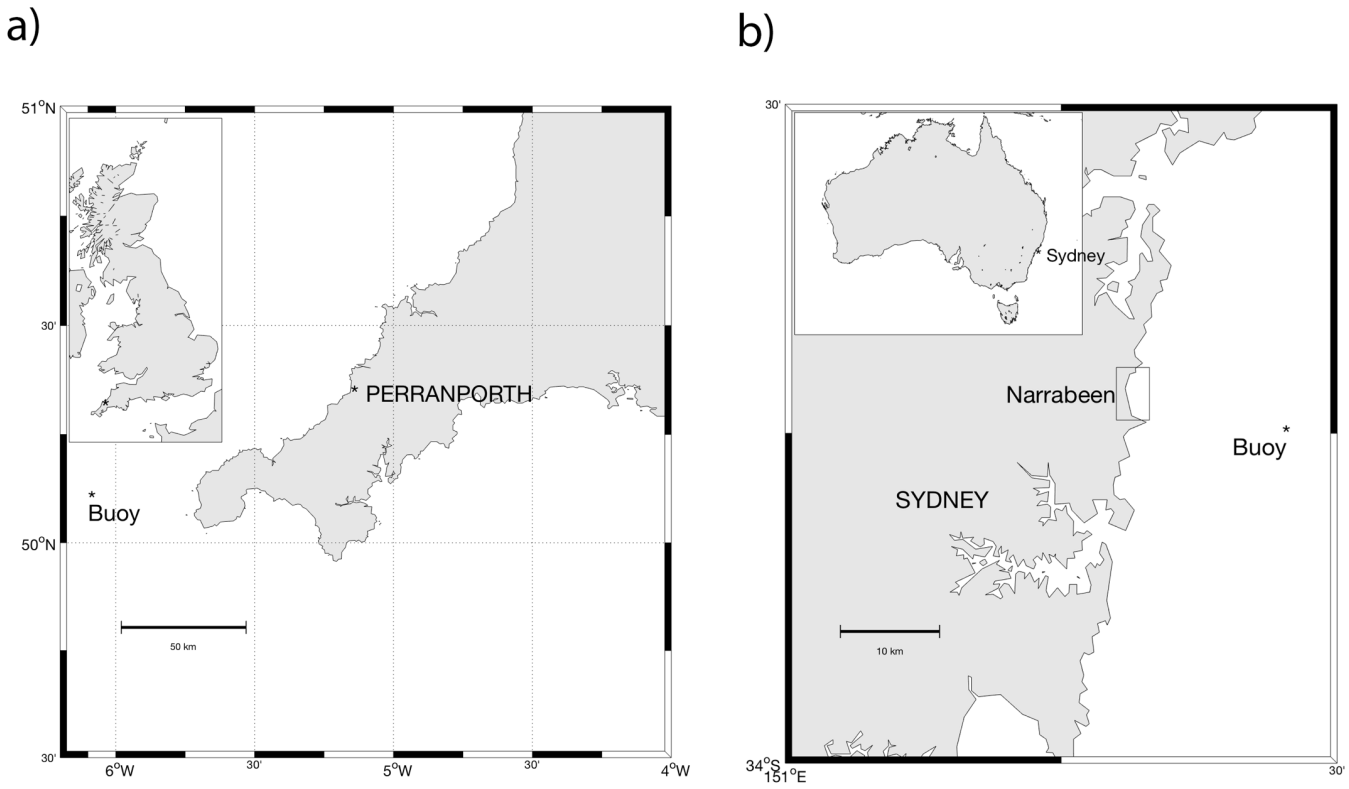

Figure 1. Location map for a) Perranporth, Cornwall, UK and b) Narrabeen, NSW, Australia.

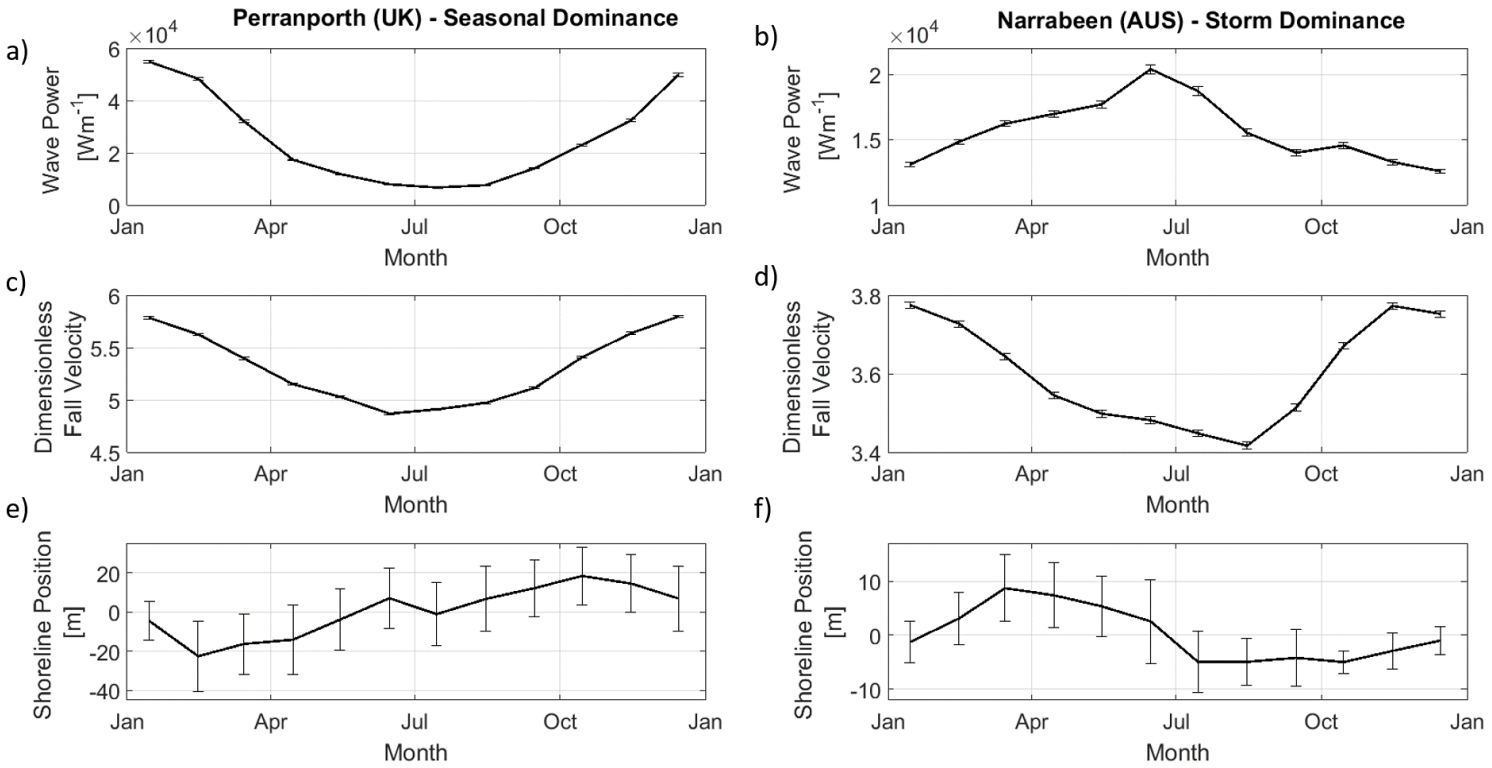

Figure 2. Monthly ensemble averages offshore wave power (top), dimensionless fall velocity (middle) and shoreline displacement (bottom) for Perranporth, UK (left) and Narrabeen, Australia (right). Ensemble means are presented with 95% confidence interval bars in all cases. The number of years of wave data in the ensembles for Parranporth and Narrabeen are 63 and 36 years respectively. For both sites over 8-years of shoreline data have been ensemble averaged.

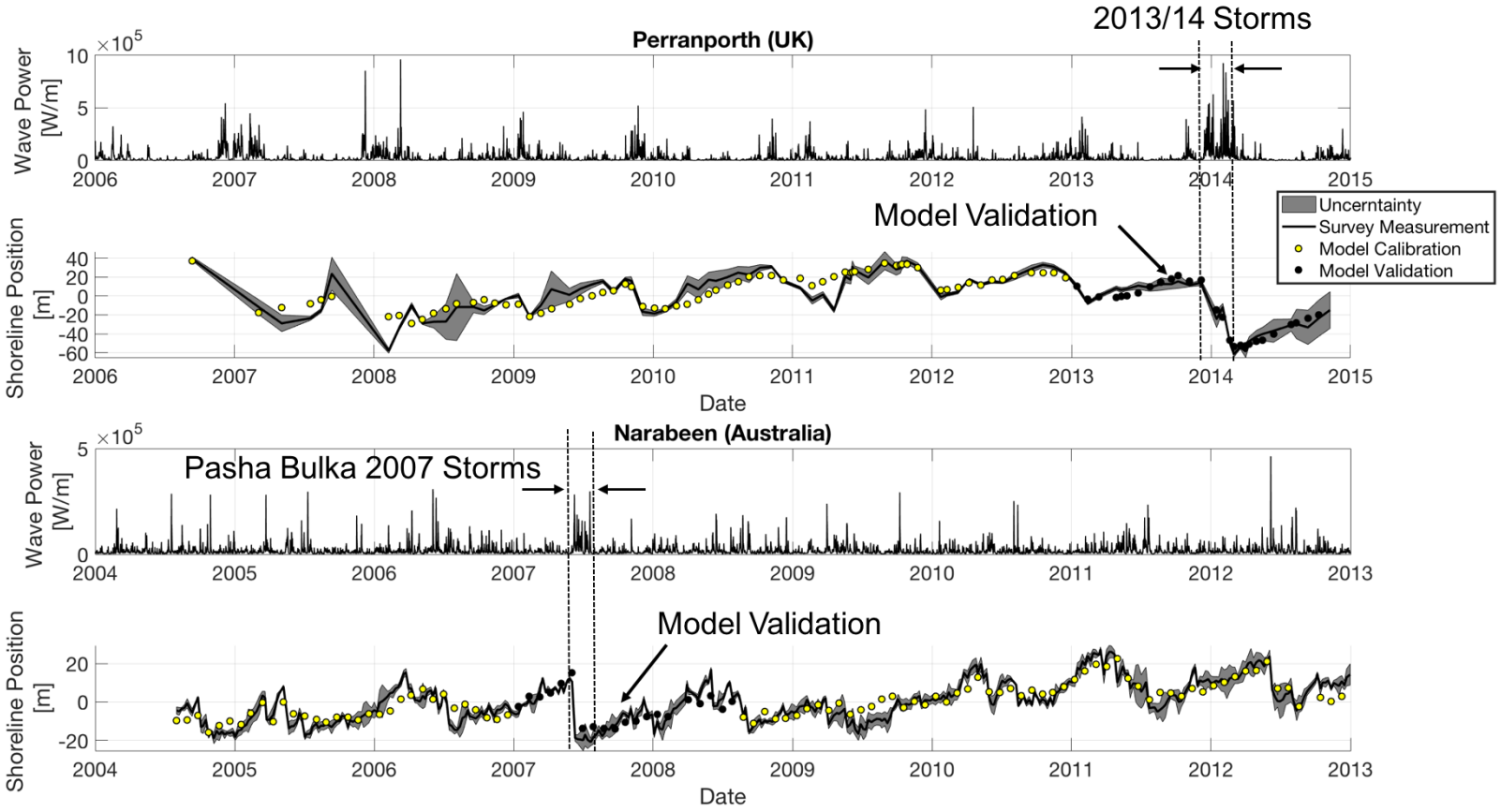

Figure 3. The top two plots (a and b) show the 9-year wave power and associated shoreline displacements (mean high-tide contour) recorded at Perranporth. Also shown are the model calibrations hindcasts and the unseen storm-validation hindcasts for the 2013/14 storms. The lower two plots are the equivalent series for Narrabeen (c and d). Notice that the Pasha Bulker June 2007 storm series has been used for the unseen model validation.

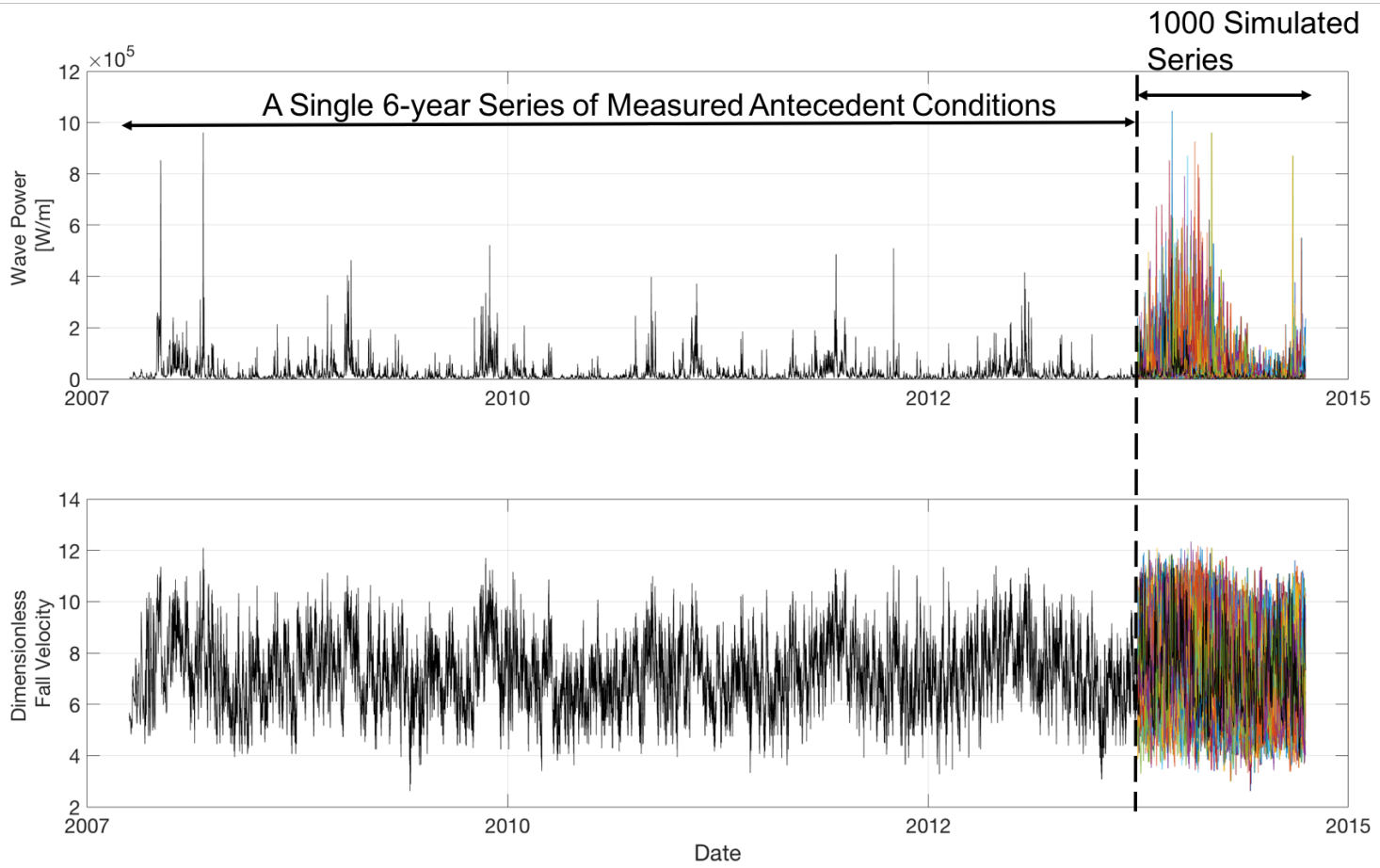

Figure 4. An example of the synthetic forcing time-series (wave power [top] and dimensionless fall velocity [bottom]) used to drive the shoreline forecast. This is an annual forecast starting on the 1st October 2013 (dotted vertical line). Noticed that each record starts with 6-years of observed antecedent measurements to which 1000 different, year-long, synthetic series are appended.

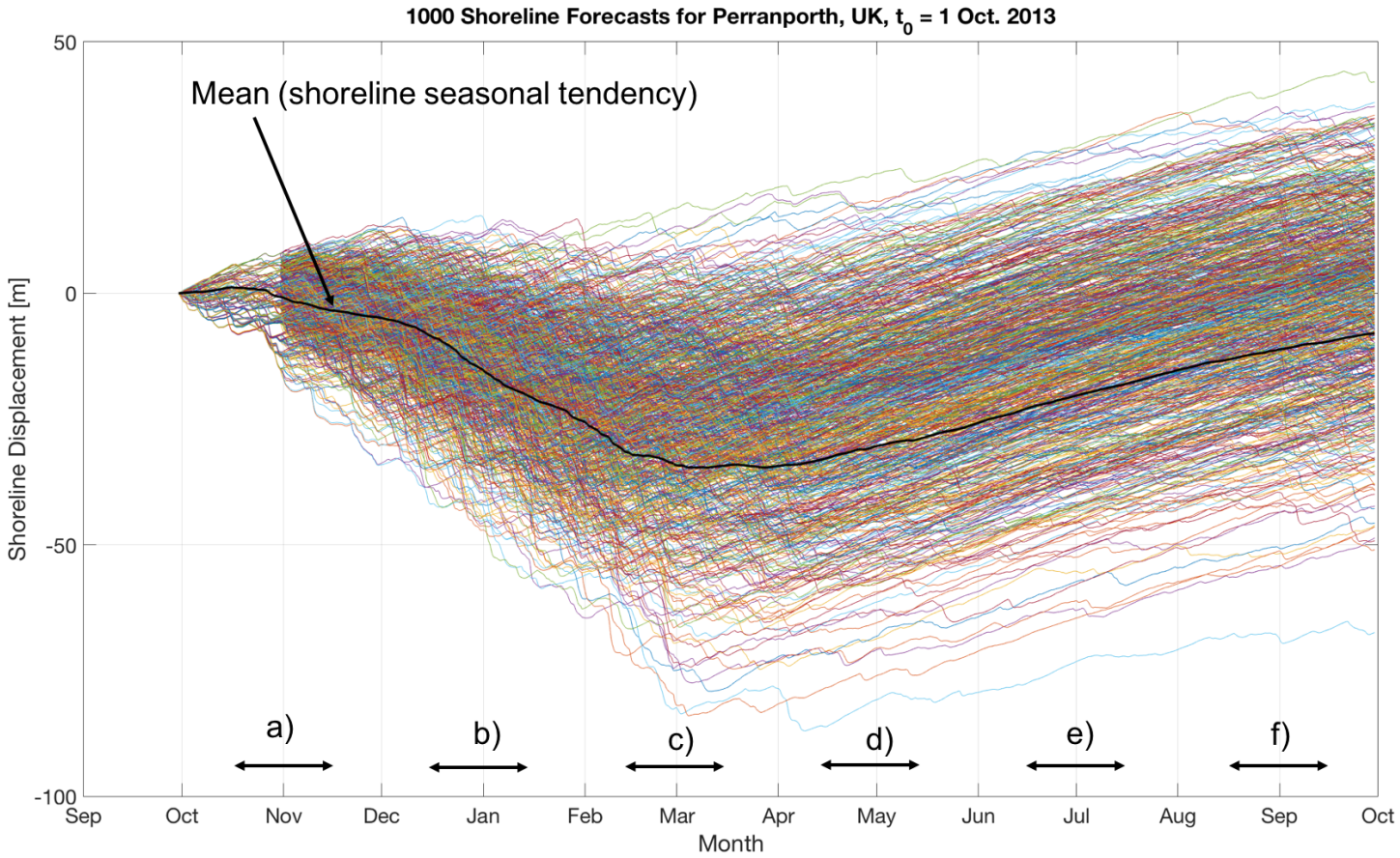

Figure 5 This figure shows the 1000 resulting shoreline estimates generated from applying the forcing series in figure 4 to the ShoreFor model. The ensemble-mean tendency is shown by the solid black line, illustrating the seasonal trend in shoreline erosion and accretion. The letters and arrow represent the shoreline data shown in the figures 6 a to f. ($Pr_{threshold}$=1/12)

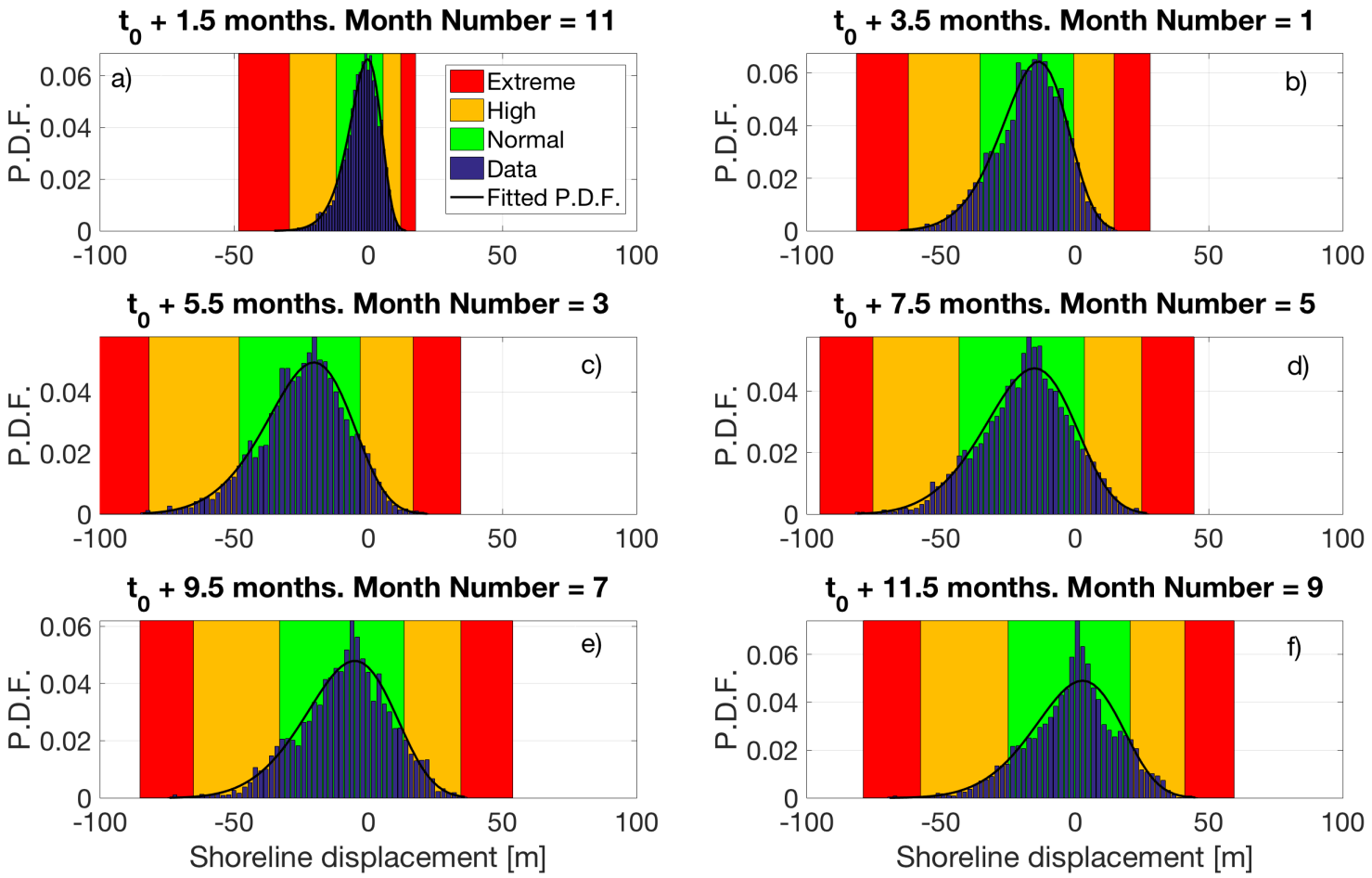

Figure 6. Histograms of the shoreline data for different months after the start of the forecast t_0 =1 October 2013. All shoreline positions are relative to the starting location at t_0. Also shown is the extreme value analysis probability density function fitted to the data (solid black line). The traffic light system represents the normal (green), high (amber) and extreme range (red). ($Pr_{threshold}$=1/12).

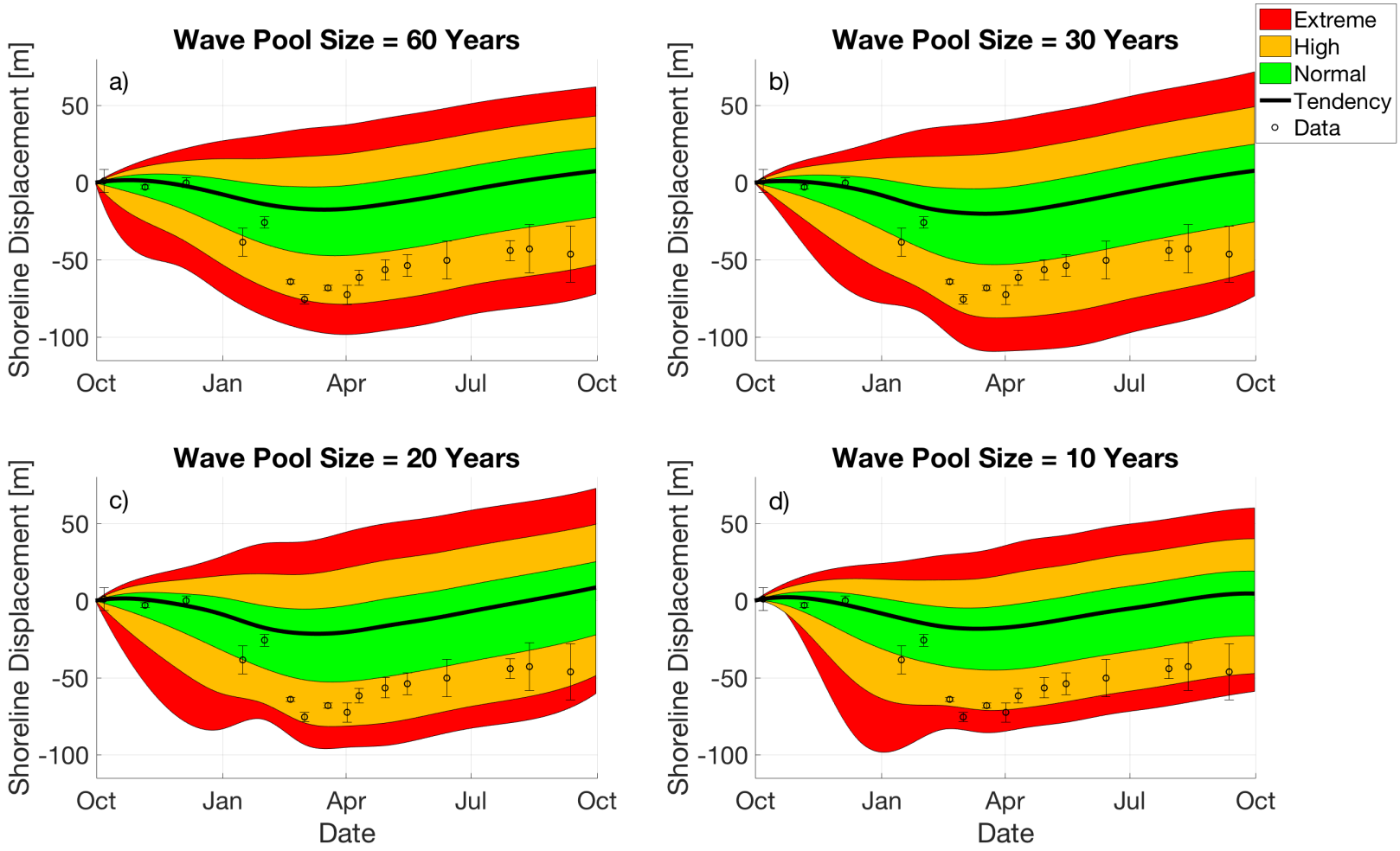

Figure 7. Sensitivity analysis on the duration of the wave pool used to generate the synthetic wave time-series. Data are shown with error bars representing +/- two standard deviations in the 400m longshore shoreline contour, which have need averaged to give the shoreline estimates [open circles]. Notice that the classification of the storm remains unchanged until the wave pool is decimated to 10-years. ($Pr_{threshold}$=1/12)

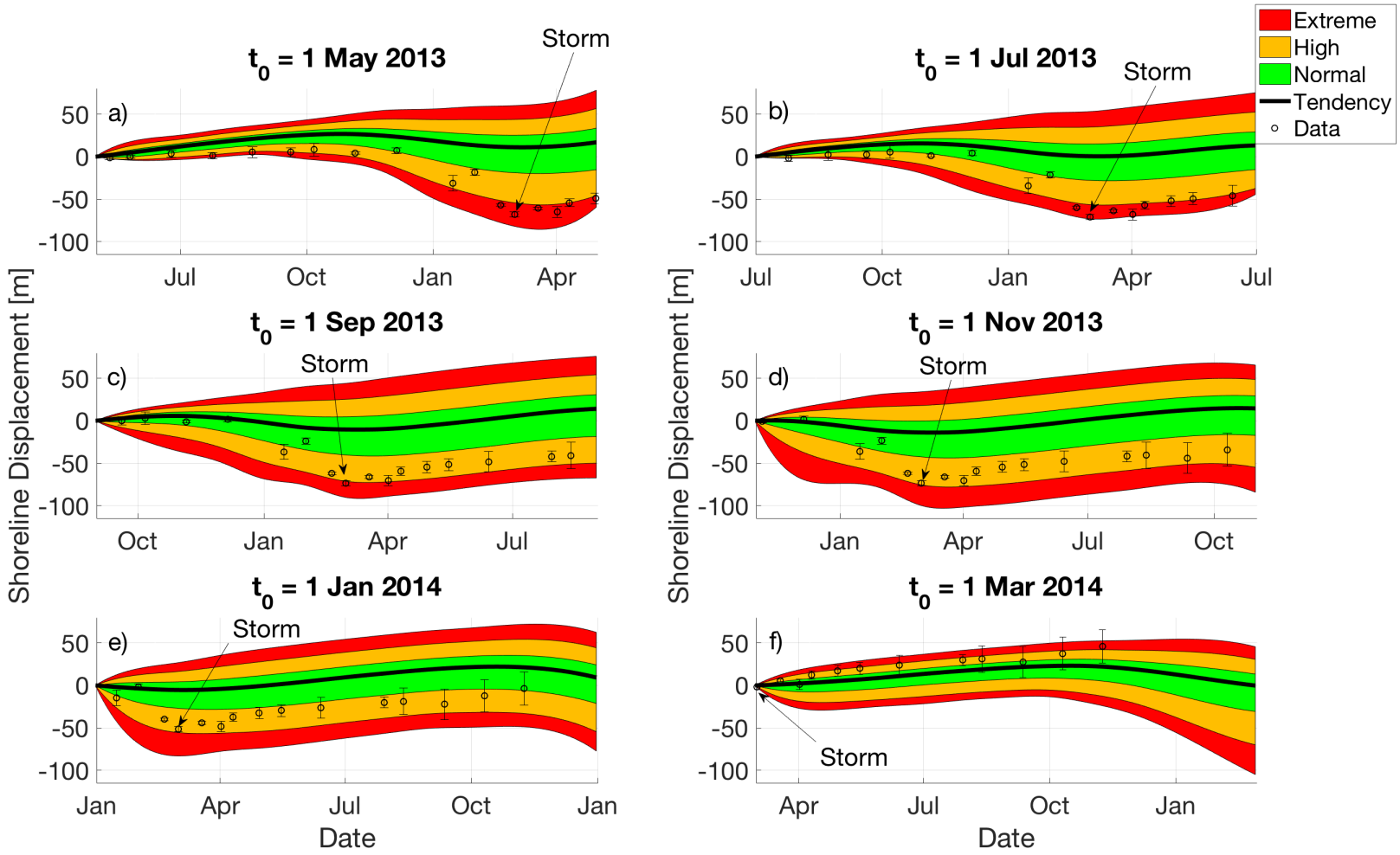

Figure 8: Six forecasts of shoreline displacements for Perranporth Beach, UK (seasonally dominated system), starting during the pre-storm recovery period in May and progressing in 2-mothly intervals until the post-storm recovery period in March 2014. The arrow indicates the maximum shoreline recession due to the storm in each case. ($Pr_{threshold}$=1/12).

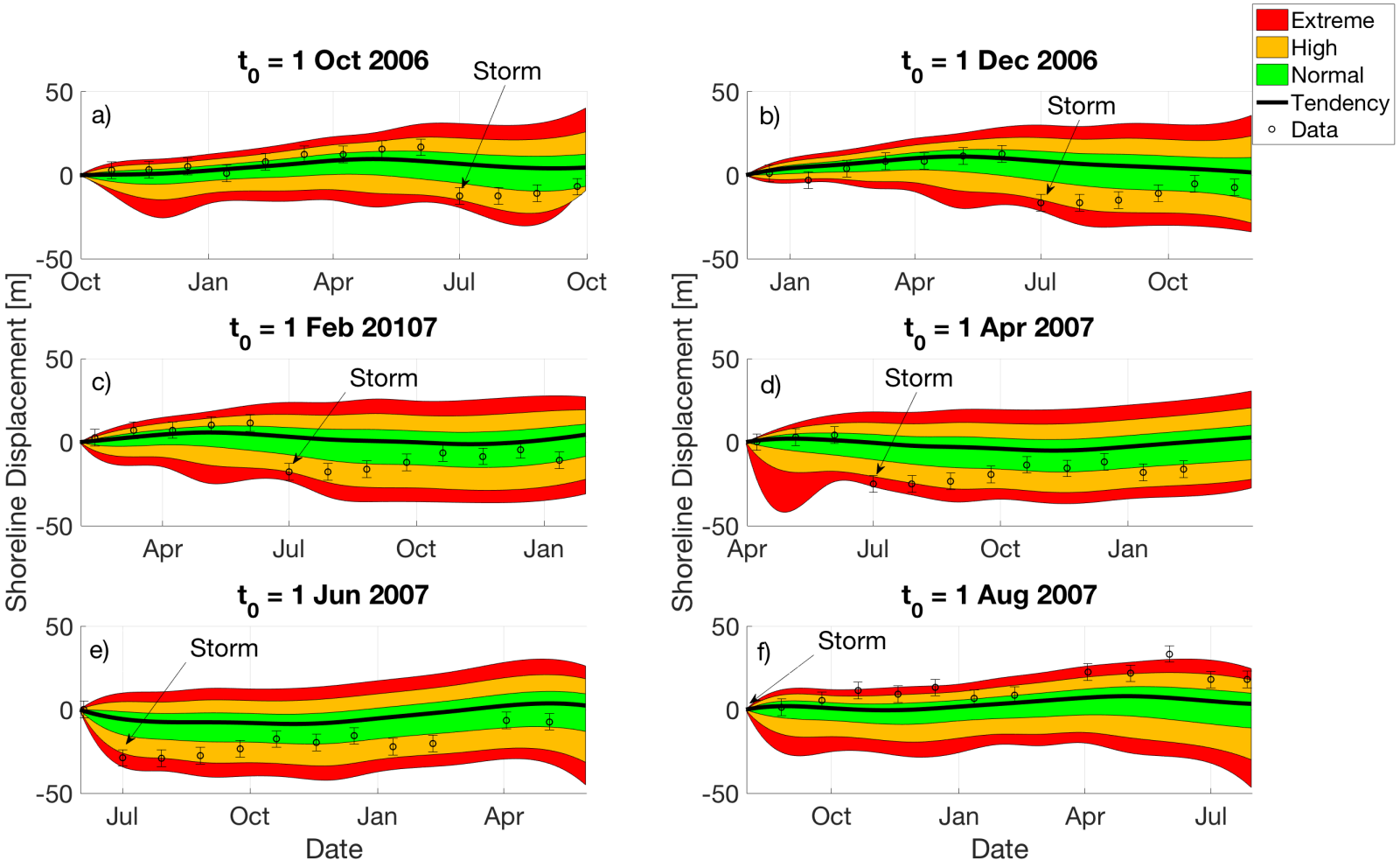

Figure 9 Forecasted shoreline response for Narrabeen, Australia (storm dominated system). Forecasts start with t_0 at the pre-storm recovery phase in October 2006 and progress at two-monthly intervals through the main storm sequence in June 2007 and to the post-storm recovery starting in August 2007. ($Pr_{threshold}$=1/12).

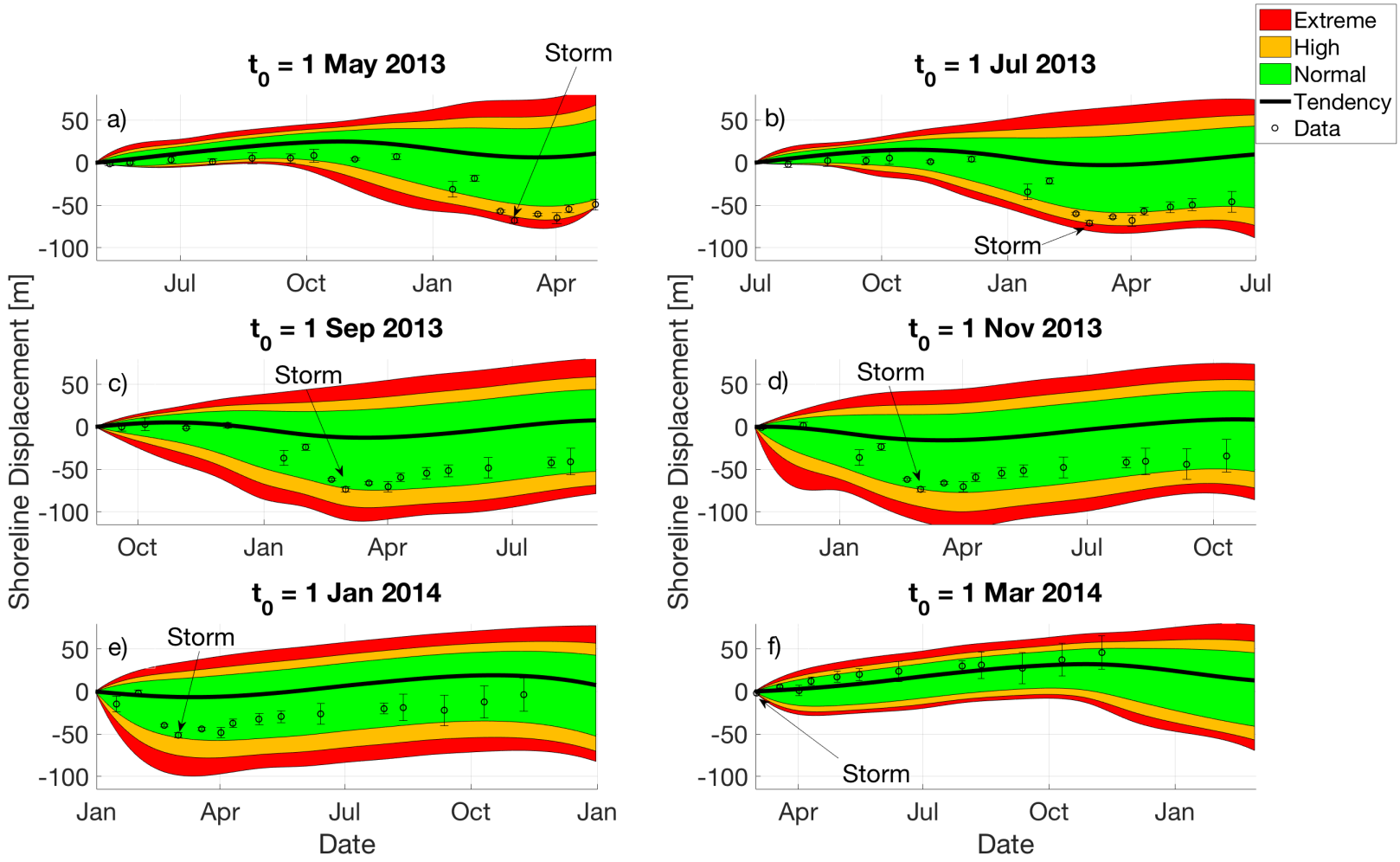

Figure 10. Similar Perranporth example plot to Figure 8 with a modified event probability threshold of $Pr_{threshold}$=1/365.

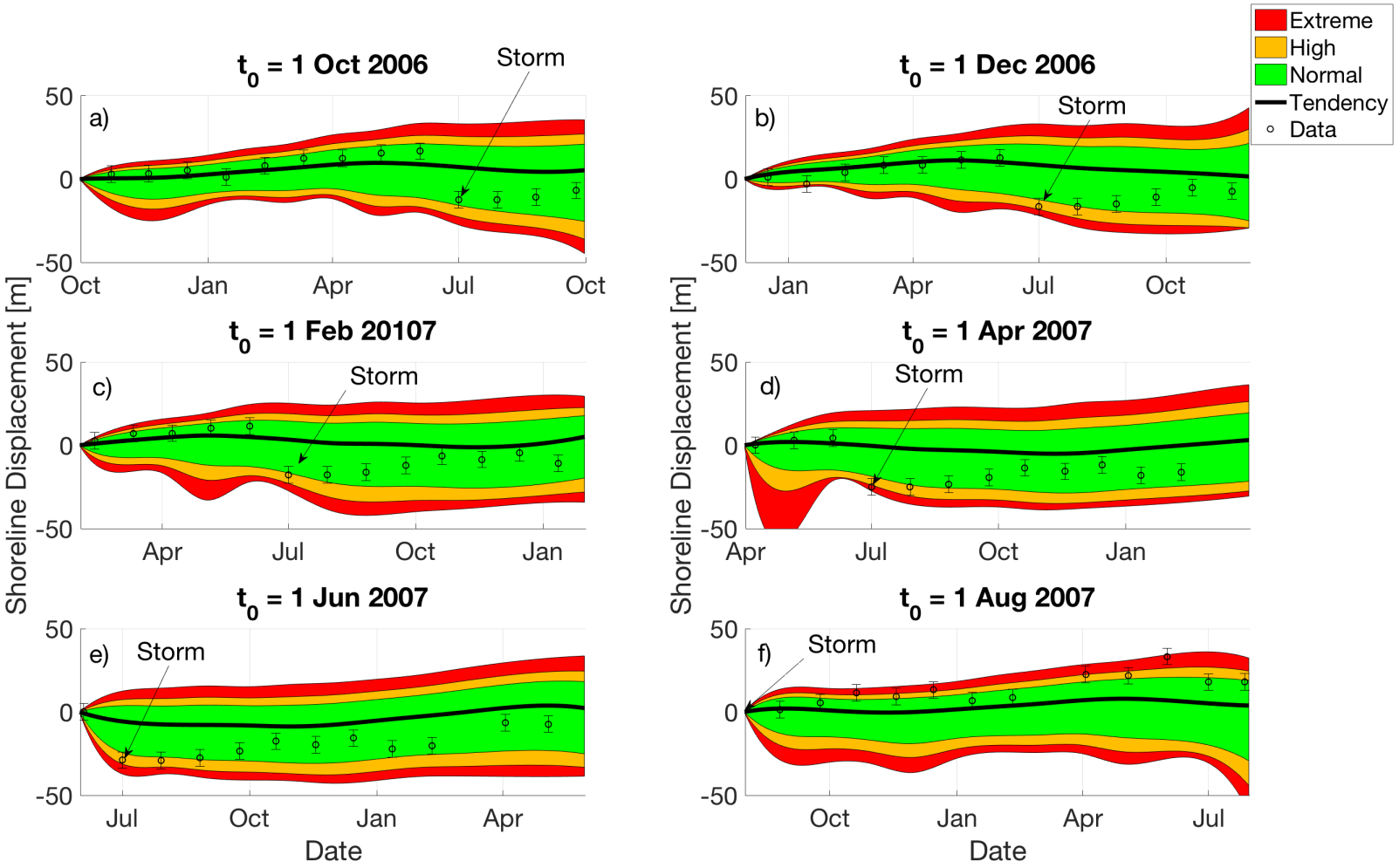

Figure 11. Similar Narrabeen example plot to Figure 9 with a modified event probability threshold of $Pr_{threshold}$=1/365.